Journal of Solid State Chemistry 183 (2010) 2669–2674

Contents lists available at ScienceDirect

Journal of Solid State Chemistry

journal homepage: www.elsevier.com/locate/jssc

In-situ synthesis of magnetic ($NiFe_2O_4$/CuO/FeO) nanocomposites

Manish Srivastava [a], Animesh K. Ojha [b,*], S. Chaubey [a], Jay Singh [c]

[a] Department of Physics, Motilal Nehru National Institute of Technology, Allahabad 211004, India
[b] School of Engineering and Science, Jacobs University, 28759 Bremen, Germany
[c] Department of Chemistry, Motilal Nehru National Institute of Technology, Allahabad 211004, India

ARTICLE INFO

Article history:
Received 14 May 2010
Received in revised form
18 August 2010
Accepted 30 August 2010
Available online 8 September 2010

Keywords:
Nanocomposites
Sol–gel
TEM
Magnetic properties

ABSTRACT

In-situ synthesis of magnetic nanocomposites with ($NiFe_2O_4$/CuO/FeO) crystal phases has been done using a sol–gel method by taking a non-stoichiometric composition of the precursors. The average particle size of the nanocomposites was calculated using X-ray diffraction (XRD) and high resolution tunneling electron microscope (HR-TEM) and it turns out to be ~20 nm. The vibrating sample magnetometer (VSM) measurements demonstrate the ferromagnetic nature of the nanocomposites. The synthesized nanocomposite was used to prepare magnetic fluid using tetramethylammonium hydroxide as a surfactant and its stability in the solution was also discussed.

1. Introduction

In recent years, the nano size materials have attracted considerable attentions due to their unique mechanical, physical, optical, and magnetic properties [1–6]. The unique properties of the nano size materials stimulate several applications in different technological fields such as electronics, catalysis, magnetic data storage, energy storage, structural components, and ceramics [7,8]. Many studies can be found in the literature on the synthesis and characterization magnetic nanomaterials. However, the studies on nanocomposites magnetic materials will be of great interest due to their tailor-made properties for both, fundamental magnetic investigation and engineering applications. The nanocomposite constitutes with the variety of distinctly different materials mixed at the nanometric scale. Different types of magnetic nanocomposites such as; MFe_2O_4/Co (*M*=Fe, Mn), where Co and MFe_2O_4 was taken as core and shell, respectively [9], $CuFe_2O_4/CeO_2$ [10], $CoFe_2O_4$-PPy [11], Fe_3O_4-ZnO [12], ferrimagnetic-metal alloys [13] and ferrimagnetic-zeolite [14] have been reported.

Among the various applications of the magnetic nanomaterials the ferrofluids (FFs)/or magnetic (nano) fluids (M(N)Fs) and magnetorheological fluids (MR fluids, MRFs) have numerous applications in different areas such as sensors, stepper motors, emission control seals, design and fabrication of a magnetic micro fluidic light modulator, loudspeakers, liquid seals around the spinning drive shafts in hard disks, tunable optical filters, cancer detection, biology, medical diagnosis and therapy, and heat transfer in electrical power plants [15].

Several studies on the synthesis and characterization of various types of magnetic ferro-fluid/magnetorelogical fluid (FFs/MR) and thermo-responsive magnetic colloids have been reported [16,17]. Nedkov et al. [18] have reported the ferrofluids based on two types of hybrid particles, Fe_3O_4/b-cyclodextrin using mono-domain (below 60 nm) magnetite nanoparticles with non-super-paramagnetic and with superparamagnetic (SPM) behavior. The effects of hyperthermia in the ferrofluids were studied. The colloidal stability of the fluids was achieved using tetramethylammonium hydroxide (TMAOH) as a surfactant and b-cyclodextrin (b-CD) as outer shell for the conjugated particles. The sedimentation and magnetorheological properties of magnetorheological (MR) fluids based on CNT/Fe_3O_4 nanocomposites were also studied [19]. The MR fluids based on CNT/Fe_3O_4 nanocomposites exhibit high sedimentation stability and obvious magnetorheological behaviors such as an apparent viscosity depending on the applied field. These predominant properties were explained in terms of soft magnetic layer covering the outside of the hollow CNTs and the large length–diameter ratio of the nanocomposites. The mechanism of chain formation in ferrofluid based MR fluid which was quite different from conventional MR fluid had been also reported [20].

The wide applications of nanocomposite materials have lead to the development of various synthesis methods such as sol–gel, co-precipitation, microemulsion, arc-discharge technique, pulsed laser ablation, ball milled, and RF-sputtering. In particular, the sol–gel method is one of the most useful and attractive techniques for the

* Corresponding author. Fax: +91 532 2545341.
E-mail addresses: animesh_r1776@rediffmail.com, animesh@mnnit.ac.in (A.K. Ojha).

0022-4596/$ - see front matter © 2010 Elsevier Inc. All rights reserved.
doi:10.1016/j.jssc.2010.08.037

preparation of nano size particles because of its advantages such as good stoichiometric control and the production of ultrafine particles with a narrow size distribution. In the present work, we have synthesized metal-oxide/ferrite nanocomposites using the modified compositions of the precursors in the basic medium using the sol–gel method. A similar kind of synthesis has been also reported in our earlier studies [21,22]. However, in those studies, the size of the particles generated was considerably large (more than 100 nm) and there distribution was not uniform. In this report, we have synthesized relatively smaller size (~17 nm) nanocomposites and their physical properties have been investigated. Its application as a magnetic fluid has been also done.

2. Experimental

2.1. Synthesis of magnetic nanocomposites

The synthesis protocol of the nanocomposites powder is similar to our earlier study [21]. According to the composition, $CuNi_{1-x}Fe_xO_y$ (x=0.2, 0.4, 0.5, and 0.8) the appropriate amounts of metal nitrates and glycolic acid were first dissolved into deionized water to form a mixed solution of the metal salts. The molar ratio of metal nitrates to glycolic acid was taken as 1:2.5. The pH value of solution was adjusted to ~8 using 25% aqueous solution of ammonia. Further, the mixed solution was heated at 70–80 °C to remove extra amount of water and to get a transparent sol. The sol was further heated at 80–90 °C under the constant stirring process to obtain viscous gel. The obtained gel was calcined at 500 °C for 10 h to get the final product.

2.2. Synthesis of magnetic fluid

To obtain a stable magnetic fluid, the synthesized nanocrystallites were coated with tetramethyl-ammonium hydroxide. The magnetic nanoparticles were dispersed in tetramethyl ammonium hydroxide under vigorous stirring process and, further the mixture was centrifuged at 12000 rpm for 20 min to remove aggregates, if any. Tetramethyl ammonium hydroxide coated magnetic nanoparticles were further dispersed in water in order to get the magnetic fluid.

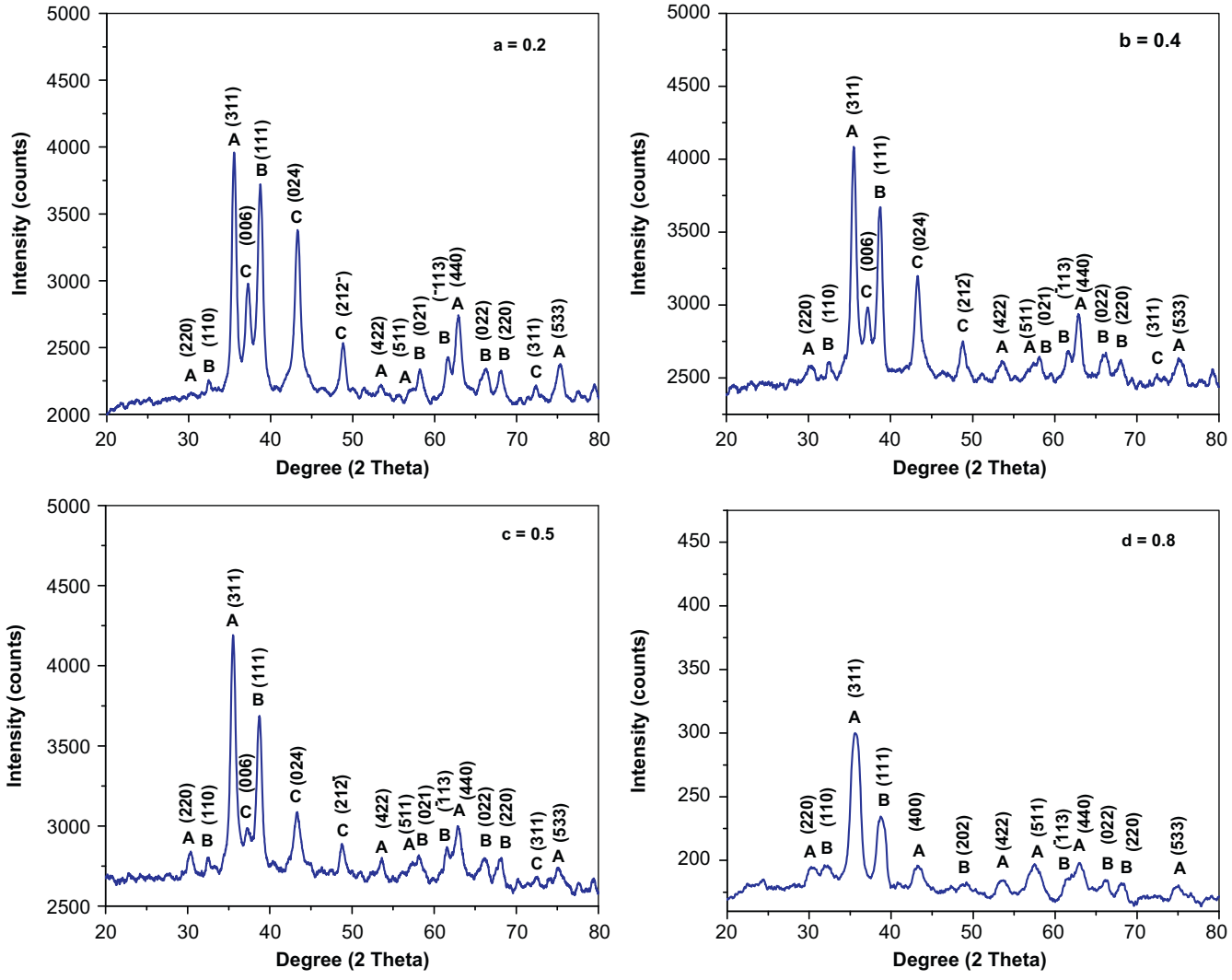

Fig. 1. XRD pattern of $CuNi_{1-x}Fe_xO_y$ nanocomposites synthesized at different iron concentrations (x=0.2, 0.4, 0.5 and 0.8) and the peaks mark as A, B, C represent the planes corresponding to three different phases $NiFe_2O_4$, CuO, and FeO phases, respectively.

2.3. Characterizations

The structural analysis of the synthesized samples was carried out by X-ray diffraction (XRD), XPERT-PRO (PW3050/60), powder diffractometer equipped with a copper target and nickel filter. X-ray wavelength, 0.15406 nm of Cu$K\alpha$ operated at 30 kV and 30 mA was used. High resolution transmission electron microscope (HR-TEM) images and selective area electron diffraction (SAED) pattern of the nanoparticles were recorded on Technai G^2 S-Twin electron microscope. The hysteresis loop, saturation magnetization and coercivity of the nanocomposites were measured by VSM (ADE-DMS, model EV-7USA) at a maximum applied field of 1.75 T at room temperature.

3. Results and discussion

3.1. XRD

The XRD patterns of the synthesized nanocomposites are shown in Fig. 1(a–d). The diffraction peaks corresponding to the planes (220), (311), (400), (422), (511), (440), and (533) confirm

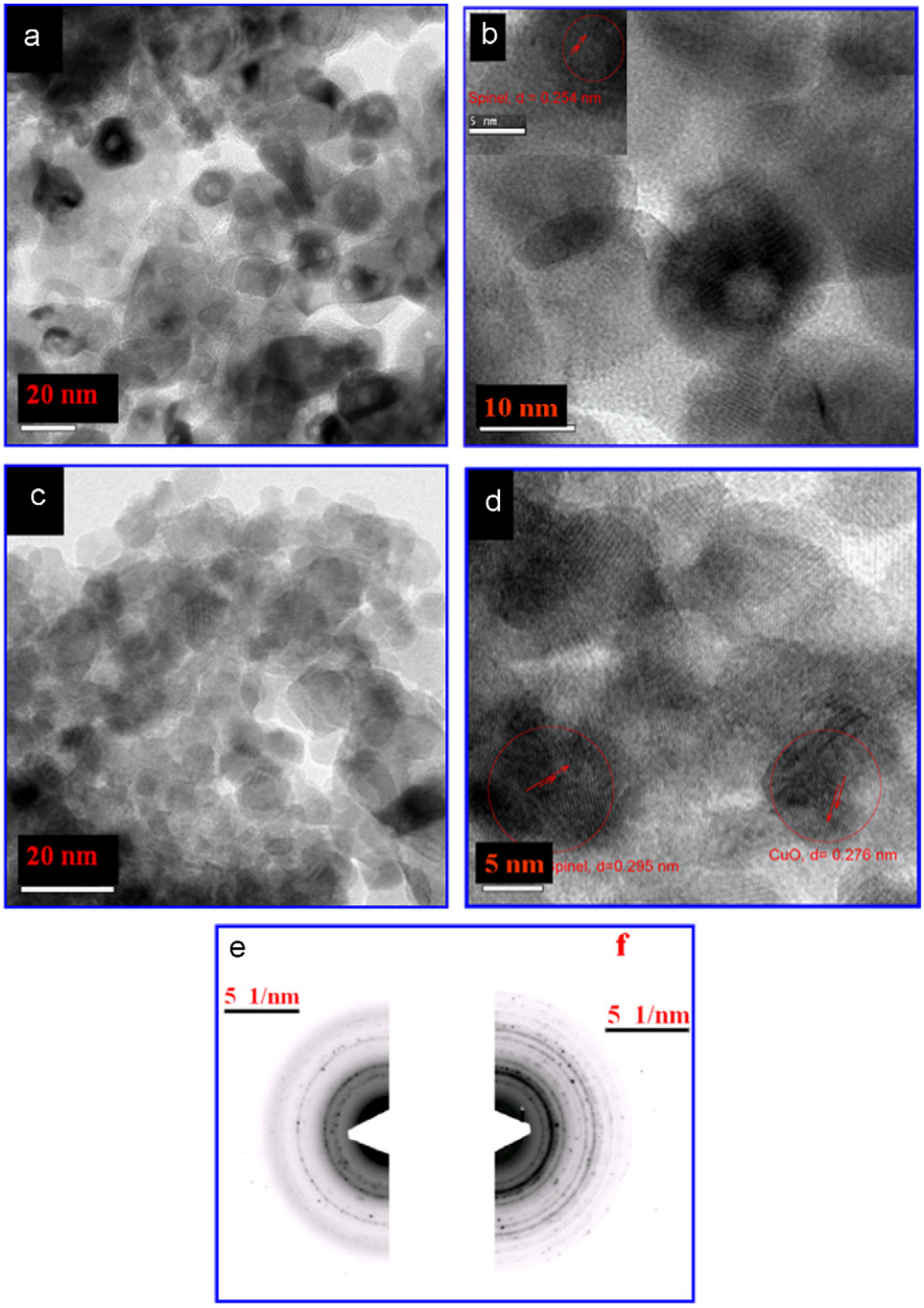

Fig. 2. (a) TEM micrograph, (b) HR-TEM image of the $CuNi_{0.8}Fe_{0.2}O_y$ nanocomposite and inset (bar length 5 nm) is the selected area showing the planes for $NiFe_2O_4$ phase with a lattice spacing of 0.254 nm, (c) TEM micrograph, (d) HR-TEM image of the $CuNi_{0.2}Fe_{0.8}O_y$ nanocomposite and selected area showing the planes with a lattice spacing of 0.295 and 0.276 nm corresponding to $NiFe_2O_4$ and CuO phases, respectively, (e) SAED pattern of $CuNi_{0.8}Fe_{0.2}O_y$, and (f) $CuNi_{0.2}Fe_{0.8}O_y$ nanocomposites.

the formation of $NiFe_2O_4$ (A) phase [21,22]. However, the peaks corresponding to the planes (110), (111), (202), ($\bar{1}$13), (022), (024), (006), and (21$\bar{2}$) show the formation of CuO (B) [23] (JCPDF-80-1268) and FeO (C) (JCPDF-89-0690) phases, respectively. The crystallite size, D is calculated for the most intense peak corresponding to the (311) plane using the Scherrer formula [24]:

$$D = (0.9\lambda)/(\beta\cos\theta) \quad (1)$$

where λ is the wavelength of the target Cu$K\alpha$ 1.54060 Å, β is the full width at half maximum corresponding to the diffracted (311) plane. The crystalline size was also calculated using other planes, (220) and (440) which provide similar kind of conclusions as we have derived from (311) plane. The crystalline size of the nanocomposites was found to vary between 16 and 20 nm.

3.2. TEM analysis

The crystallinity, particle size, and structural morphology of the synthesized nanocomposites were investigated using TEM, HR-TEM, and SAED images. The TEM image of the synthesized nanocomposites presented in Fig. 2(a and c) shows that the particles are approximately spherical in shape and their size (diameters) was found to be in the range of 10–25 nm. The HR-TEM image (see Fig. 2(b and d)) confirms the presence of CuO and $NiFe_2O_4$ phases. In $NiFe_2O_4$ phase, the 'd' value corresponding to (220) plane was found to be 2.95 Å and for CuO phase corresponding to (110) plane was found to be 2.76 Å. This observation also confirms the composite nature of the synthesized nanoparticles. SAED patterns of the nanocomposites shown in Fig. 2(e) and (f) depict well-defined rings and spots, which may be attributed to the composite and polycrystalline nature of the synthesized materials [22, 25–27].

The distribution of the particles size obtained through the TEM micrograph is shown in Fig. 3(a, b). In order to analyze the size distribution quantitatively, the particle size distribution was fitted using a log-normal function [28]:

$$P(D) = \frac{A}{D\sigma_D\sqrt{2\pi}}\exp\left(-\frac{1}{2\sigma_D^2}\ln^2\left(\frac{D}{D_0}\right)\right) \quad (2)$$

where σ_D, the standard deviation of the diameter and D_0 is the mean diameter. A mean diameter D_0, of 19.13 ± 1.02 and 17.47 ± 0.84 nm was obtained for the nanocomposites synthesized at the iron concentration (x=0.2 and 0.8), respectively, using Eq. (2), showing a good agreement with the crystallite size calculated through XRD.

3.3. Magnetic properties

The magnetization curves of the synthesized nanocomposites obtained from the room temperature VSM measurements are presented in Figs. 4(a–d) and 5. The hysteresis curves show small area which is a typical feature for soft magnetic materials. It can be seen from Fig. 4(a–d) that there is non-attainment of saturation magnetization even at the high magnetic field of 1.75 T. The values of saturation magnetization (M_s), remanent magnetization (M_r), and coercivity (H_c) for the synthesized nanocomposites have been presented in Table 1. It is quite obvious from data reported in Table 1 that the value of (M_s) increases by increasing the iron concentration from x=0.2 to 0.8. This may be due to the formation of more ferrimagnetic ($NiFe_2O_4$) phases at higher iron concentrations. Non-saturated magnetization even at high fields can be attributed to the existence of small nanoparticles those have a core–shell morphology consisting

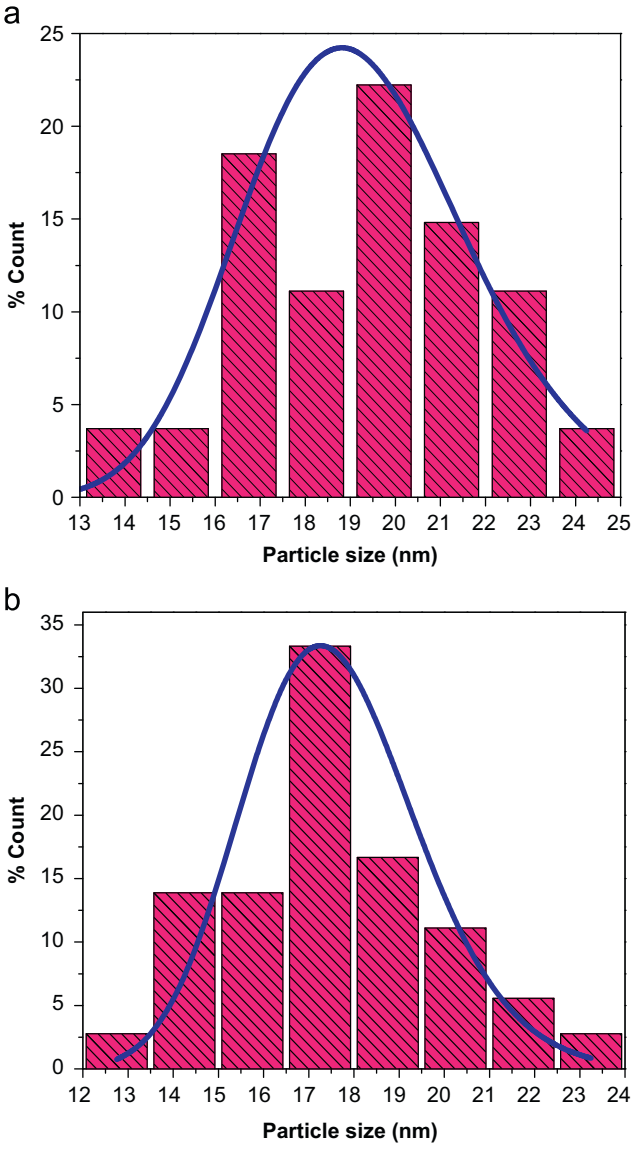

Fig. 3. (a) Particle size distribution curve for $CuNi_{0.8}Fe_{0.2}O_y$ and (b) $CuNi_{0.2}Fe_{0.8}O_y$ nanocomposites.

of ferri-magnetically aligned core spins and a spin-glass like surface layer [29–31]. In the absence of surface, the magnetization of the particles would have saturated by enhancing the value of applied magnetic field. The coercivity, (H_c) of a magnetic material is a measure of its magnetocrystalline anisotropy. The small size nanoparticles show very small hysteresis (low coercivity) and, therefore, they have a small value of anisotropy. Also, at high temperature regime, the thermal energy overcomes the anisotropy energy and therefore the synthesized nanoparticles exhibit small area (area of the loop) along with non-saturated hysteresis loop.

3.4. Magnetic fluid

Fig. 6 (i (a and b)) shows the dispersion of magnetic nanocomposites in water without and with the coating of tetramethylammonium hydroxide, respectively. It was observed that the dispersion of magnetic nanocomposites without coating of tetramethylammonium hydroxide shows low stability, while

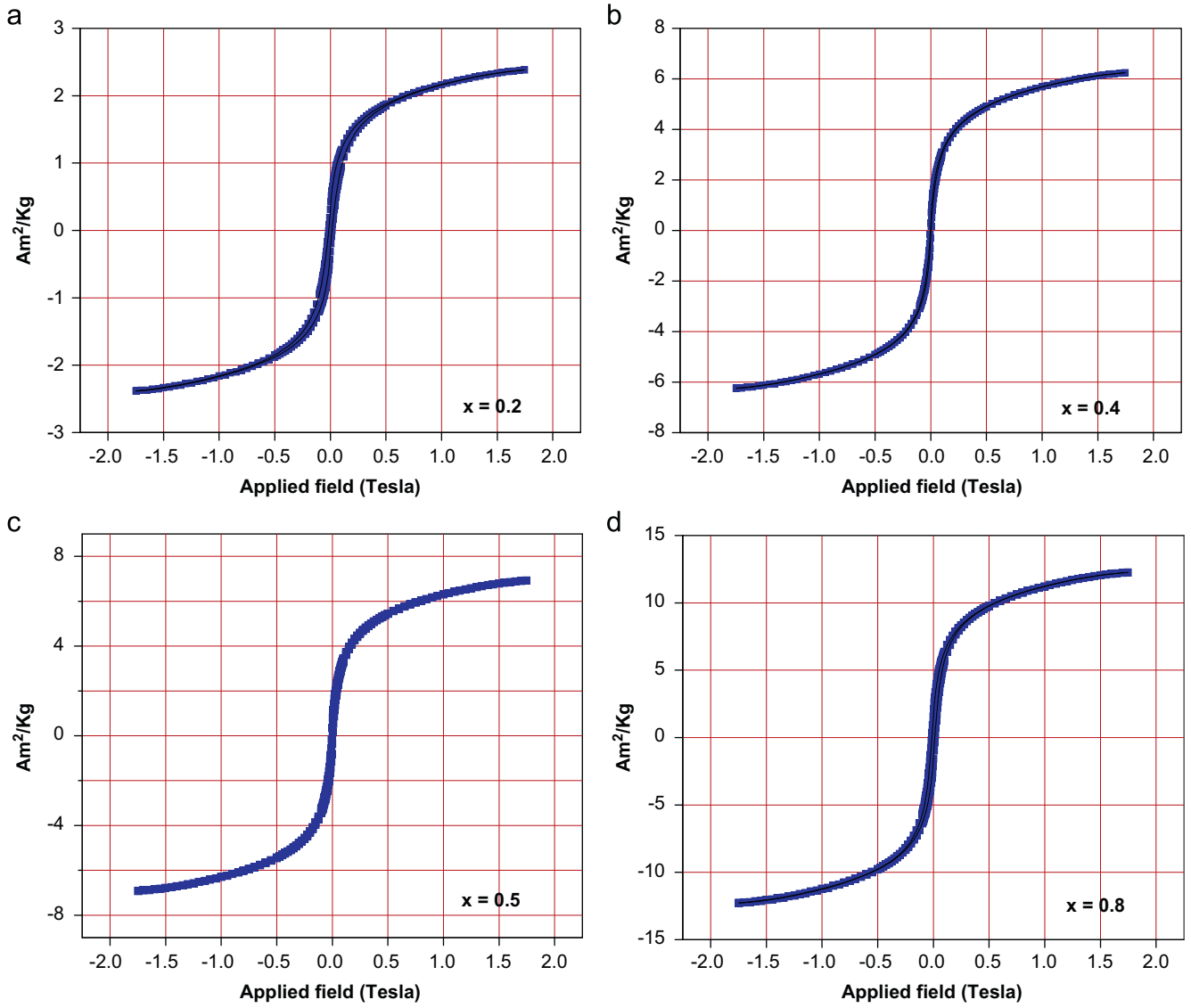

Fig. 4. (a–d) Magnetization curves of $CuNi_{1-x}Fe_xO_y$ nanocomposites synthesized at different iron concentrations (x=0.2, 0.4, 0.5, and 0.8).

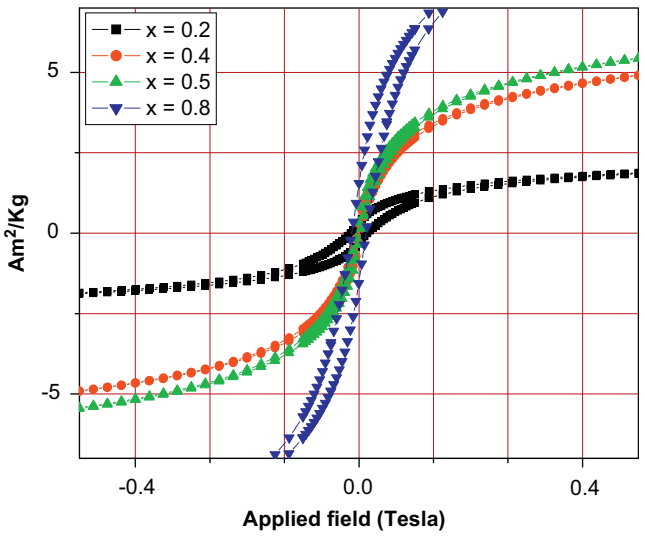

Fig. 5. Magnetization curves of $CuNi_{1-x}Fe_xO_y$ nanocomposites up to the applied field of 0.5 T, which clearly showing the presence of hysteresis loop.

the nanocomposites coated with tetramethylammonium hydroxide shows a good dispersibility. Actually, the formation of magnetic fluid involves various types of forces that hold the different components together. On the molecular level, magnetic nanoparticles are held together by ionic interactions. The tetramethylammonium [$(CH_3)_4N^+$] and hydroxide ion (^-OH) are covalent molecules and held together by the ionic interactions. The hydroxide anions adhere to the surface of magnetic particles and these negative charges attract their counter ions such as tetramethylammonium cations, forming a positively charged outer shell. Since like charges repel, the electrostatic repulsion between positively charged outer shells prevent magnetite particles from the agglomeration and causing magnetic nanoparticles to exist in the form of suspension in colloidal solution. However, without tetramethylammonium hydroxide, the magnetic nanoparticles tend to aggregate due to the Van-der Waals interaction. Therefore, it is critical to have the appropriate surfactant to stabilize an aqueous magnetic fluid. The mechanism of the formation of colloidal suspension is shown in Fig. 6(ii). Fig. 6(i (c and d)) shows the separation and re-dispersion process of the magnetic nanocomposites in distilled water in the absence and presence of an external magnetic field, respectively.

Table 1
The values of magnetic parameters such as M_s, M_r, and H_c of the nanocomposites synthesized at different iron concentrations.

Composition $CuNi_{1-x}Fe_xO_y$	Saturation magnetization (M_s) (A m^2/kg)	Remanent magnetization (M_r) (A m^2/kg)	Coercivity (H_c) (T)
(x=0.2)	2.380	0.312	147.5×10^{-4}
(x=0.4)	6.243	0.289	31.62×10^{-4}
(x=0.5)	6.920	0.343	34.00×10^{-4}
(x=0.8)	12.200	1.500	130.5×10^{-4}

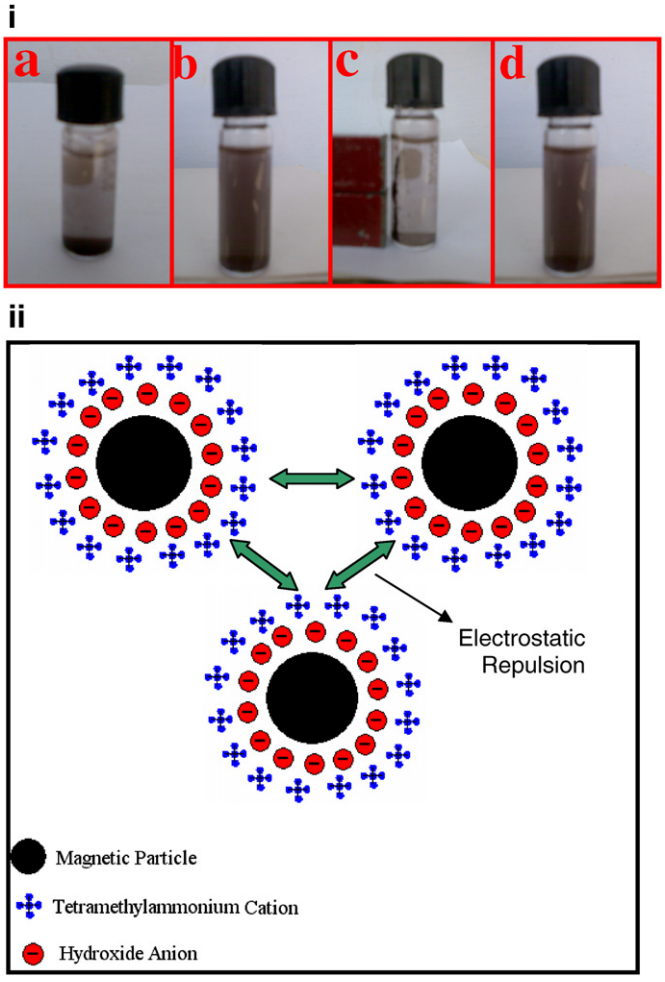

Fig. 6. (i) (a) Dispersion of magnetic nanocomposites in water without and (b) with the coating of tetramethylammonium hydroxide, (c) the separation, and (d) re-dispersion process of the magnetic nanocomposites in the distilled water (left) in the absence and (right) in the presence of an external magnetic field (ii) Mechanism of the formation of colloidal suspension.

4. Conclusions

In this study, in-situ synthesis of the nanocomposites with ($NiFe_2O_4$/CuO/FeO) crystal phases was successfully done by the sol–gel method. In order to analyze the size distribution quantitatively, the particle size distribution was fitted using a log-normal function. The average size of the nanoparticles obtained through the fitting was fond to be 19.13 ± 1.02 and 17.47 ± 0.84 nm for the nanoparticles synthesized at the iron concentrations x=0.2 and 0.8, respectively. The VSM results show the ferromagnetic nature of the nanocomposites. The synthesis of magnetic fluid using tetramethylammonium hydroxide as the surfactant has been performed and its stability behavior in the solution was also investigated.

Acknowledgments

MS is thankful to MNNIT, Allahabad for granting the research fellowship. AKO is thankful to the Alexander von Humboldt Stiftung for the award of a research fellowship. The Department of Chemistry of MNNIT, Allahabad is gratefully acknowledged for granting access to the available research facilities. We are thankful to Prashant K. Sharma and Avinash C. Pandey, Nanophosphor Application Centre, University of Allahabad for providing access to the TEM facility.

References

[1] R. Vaben, D. Stover, J. Mater. Process. Technol. 92 (1999) 77.
[2] M.S. Niasari, F. Davar, M. Mazaheri, M. Shaterian, J. Magn. Magn. Mater. 320 (2007) 575.
[3] J. Karch, R. Brringer, H. Gleiter, Nature 330 (1987) 556.
[4] M.J. Mayo, D.C. Hague, D.J. Chen, Mater. Sci. Eng. A 166 (1993) 145.
[5] M. Mayo, J. Mater. Des. 14 (1993) 323.
[6] Y. Sakka, T.S. Suzuki, K. Morita, K. Nakano, K. Hiraga, Scr. Mater. 44 (2001) 2075.
[7] A. Weibel, R. Bouchet, P. Bouvier, P. Knauth, Acta Mater. 54 (2006) 3575.
[8] S. Yang, L. Gao, J. Am. Ceram. Soc. 88 (2005) 968.
[9] S. Peng, J. Xie, S. Sun, J. Solid State Chem. 181 (2008) 1560.
[10] R.K. Selvan, C.O. Augustin, V. Sepelák, L.J. Berchmans, C. Sanjeeviraja, A. Gedanken, Mater. Chem. Phys. 112 (2008) 373.
[11] N. Murillo, E. Ochoteco, Y. Alesanco, J.A. Pomposo, J. Rodriguez, J. González, J.J. del Val, J.M. González, M.R. Britel, F.M. Varela-Feria, A.R. de Arellano-López, Nanotechnology 15 (2004) S322.
[12] J. Wan, H. Li, K. Chen, Mater. Chem. Phys. 114 (2009) 30.
[13] Y.W. Yun, S.W. Kim, G.Y. Kim, Y.B. Kim, Y.C. Yun, K.S. Lee, J. Electroceram. 17 (2006) 467.
[14] M. Arruebo, R.F. Pacheco, S. Irusta, J. Arbiol, M.R. Ibarra, J. Santamaría, M. Arruebo, Nanotechnology 17 (2006) 4057.
[15] F. El-Diasty, H.M. El-Sayed, F.I. El-Hosiny, M.I.M. Ismail, Curr. Opin. Solid State Mater. Sci. 13 (2009) 28.
[16] A.M. Schmidt, Colloid Polym. Sci. 285 (2007) 953.
[17] Ladislau Vékás, Adv. Sci. Technol. 54 (2008) 127–136.
[18] I. Nedkov, L. Slavov, T. Merodiiska, P. Lukanov, Ph. Tailhades, M. Gougeon, R.E. Vandenberghe, J. Nanoparticle Res. 10 (2008) 877.
[19] H. Pu, F. Jiang, Nanotechnology 16 (2005) 1486.
[20] R. Patel, B. Chudasama, Phys. Rev. E 80 (2009) 012401.
[21] M. Srivastava, A.K. Ojha, S. Chaubey, P.K. Sharma, A.C. Pandey, Mater. Chem. Phys. 120 (2010) 493.
[22] M. Srivastava, A.K. Ojha, S. Chaubey, P.K. Sharma, A.C. Pandey, J. Alloys Compd. 494 (2010) 275.
[23] D.P. Singh, A.K. Ojha, O.N. Srivastava, J. Phys. Chem. C 113 (2009) 3409.
[24] H.P. Klug, L.E. Alexander, in: X-ray Diffraction Procedure, Wiley Inter Science, New York, 1954, p. 504.
[25] G. Pourroy, A.V. Minguez, T. Dintzer, M.R. Plouet, J. Alloys Compd. 327 (2001) 267.
[26] S. Rana, J. Rawat, M.M. Sorensson, R.D.K. Misra, Acta Biomater. 2 (2006) 421.
[27] E. Mugnier, A. Barnabe, L. Presmanes, Ph. Tailhades, Thin Solid Films 516 (2008) 1453.
[28] T. Kim, M. Shima, J. Appl. Phys. 101 (2007) 09M516.
[29] R.N. Bhowmik, R. Ranganathan, J. Magn. Magn. Mater. 248 (2002) 101.
[30] D. Fiorani, S. Vitiocoli, J.L. Dorman, J.L. Tholence, A.P. Murani, Phys. Rev. B 30 (1984) 2776.
[31] H. Kavas, A. Baykal, M.S. Toprak, Y. Koseoglu, M. Sertkol, B. Aktas, J. Alloys Compd. 479 (2009) 49.